

Enhanced ultraviolet electroluminescence from ZnO nanowires in TiO₂/ZnO coaxial nanowires/poly(3,4-ethylenedioxythiophene)-poly(styrene-sulfonate) heterojunction

Chun-Yu Lee,¹ Jen-Yi Wang,² Yi Chou,³ Meng-Yueh Liu,¹ Wei-Fang Su,³
Yang-Fang Chen,² and Ching-Fuh Lin^{1,4,a)}

¹Graduate Institute of Photonics and Optoelectronics, National Taiwan University, Taipei 10617, Taiwan

²Department of Physics, National Taiwan University, Taipei 10617, Taiwan

³Graduate Institute of Materials Science and Engineering and Department of Materials Science and Engineering, National Taiwan University, Taipei 10617, Taiwan

⁴Graduate Institute of Electronics Engineering and Department of Electrical Engineering, National Taiwan University, Taipei 10617, Taiwan

(Received 5 November 2009; accepted 4 January 2010; published online 8 February 2010)

The ultraviolet (UV) electroluminescence (EL) from the TiO₂/ZnO coaxial nanowires (NWs)/poly(3,4-ethylenedioxythiophene)-poly(styrene-sulfonate) inorganic/organic heterostructure devices is greatly enhanced and the defect emission is significantly suppressed compared with the uncoated ZnO NW device at room temperature. The origins of the great changes in EL of ZnO NW devices are attributed to the surface modification of the sputtered TiO₂ coating and the reduction in the pinhole traps on the surface of ZnO NWs. It is found that for the optimized device, the EL intensity ratio between the band gap and defect emission can be greatly enhanced by up to about 250 times its prior level. Such ZnO NW devices with enhanced UV emission have potential applications in the highly efficient solid state emitters. © 2010 American Institute of Physics. [doi:10.1063/1.3304896]

I. INTRODUCTION

ZnO semiconductor has received tremendous attentions due to their excellent material characteristics such as the direct wide band gap (3.37 eV) and high excitonic binding energy that ensures significant excitonic emission at room temperature, leading to a variety of potential applications in optoelectronic nanodevices.¹⁻³ Unfortunately, due to a large surface-to-volume ratio, surface defect emissions play a dominant role in optical as well as electronic properties.⁴⁻⁷ To increase the performance of devices, how to suppress or eliminate the detrimental surface defect states becomes very important. In past years, surface modification/passivation has been recognized as the most efficient methods to build tailored nanomaterials using physical/chemical approaches.⁸⁻¹⁰ This method has been found to improve the performance of optoelectronic properties of ZnO nanostructures.^{7,11,12} For example, Shi *et al.*¹³ demonstrated enhanced near-band-edge emission from SnO₂-capped ZnO nanowire (NW) arrays. Additionally, Fang *et al.*¹⁴ reported the enhancement in ZnO nanowall photoconductivity induced by CdS nanoparticle (NP) modification. Richters *et al.*¹⁵ reported enhanced surface-excitonic emission in ZnO/Al₂O₃ core-shell NWs. However, these results are mainly based on optical excitation. Electrically pumped light emission from ZnO by surface modification/passivation has remained out of reach. This paper demonstrates the enhancement in ultraviolet (UV) electroluminescence (EL) from ZnO NWs/poly(3,4-ethylenedioxythiophene)-poly(styrene-sulfonate) (PEDOT:PSS) heterostructure through surface modification with TiO₂

coating. The EL intensity ratio between the band gap and defect emission can be greatly improved by about 250 times its current level. This study provides a useful approach for developing highly efficient light-emitting diodes (LEDs) in the UV region.

II. EXPERIMENTAL DETAILS

The ZnO NWs studied in this work were prepared by the hydrothermal method. To facilitate the nucleation of ZnO NW growth, a film of ZnO seeding layer was first spin-coated and annealed onto an indium tin oxide (ITO) substrate. A ZnO seeding solution containing zinc acetate dihydrate [Zn(CH₃COO)₂·2H₂O, Sigma-Aldrich, 99.999% purity], and equivalent molar monoethanolamine [NH₂CH₂CH₂OH, Sigma-Aldrich, 99.5% purity] dissolved in 2-methoxyethanol [CH₃OCH₂CH₂OH, Sigma-Aldrich, 99.8% purity].¹⁶ The concentration of zinc acetate was chosen to be 0.5 M. Following the deposition of the seeding layer, the ZnO NW array was grown in an aqueous solution containing 50 mM zinc nitrate [Zn(NO₃)₂·6H₂O, Sigma Aldrich, 98% purity] and 50 mM hexamethylenetetramine [C₆H₁₂N₄, Sigma Aldrich, 99.5% purity]. Typical growth temperature and time were 90 °C and 3 h, respectively. After deposition the NWs were rinsed in deionized water and dried in N₂. In order to make the experiment data comparable, the grown sample was cut into many parts; one part was used as a reference sample and the others were used to fabricate TiO₂-coated ZnO NWs using a sputtering system. The TiO₂-coated NWs were deposited by a sputtering system (JFC-1600, JEOL), with several different deposition times and two different deposition currents of 10 and 40 mA. The empty gaps between the individual TiO₂/ZnO coaxial NWs

^{a)}Author to whom correspondence should be addressed. Tel.: 886-2-3366 3540. FAX: 886-2-2364 2603. Electronic mail: cflin@cc.ee.ntu.edu.tw.

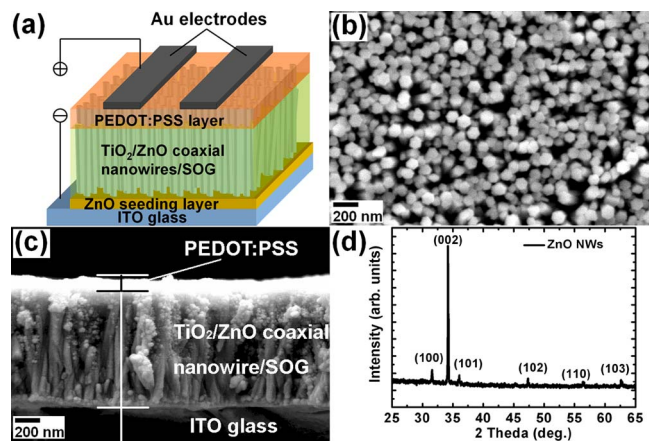


FIG. 1. (Color online) (a) Schematic illustration of the TiO_2/ZnO coaxial NWs/PEDOT:PSS heterostructure LED. (b) FESEM image of top view of ZnO NWs grown on ITO substrate. (c) Cross-sectional FESEM image of the TiO_2/ZnO coaxial NWs/PEDOT:PSS heterostructure. (d) XRD pattern of the ZnO NWs on ITO substrate prepared by hydrothermal method at 90°C for 3 h.

were filled with an insulating spin-on-glass [(SOG), a polysiloxane-based dielectric material] layer that was spin-coating from the SOG solution. Subsequently, a simple plasma etching was applied to remove the SOG coating from the top of the TiO_2/ZnO coaxial NWs to expose them for LED fabrication. We confirmed that the SOG filling was more effective than the current photoresist filling for reducing surface leakage. The hole-conducting polymer PEDOT:PSS (Baytron PH 500, H.C. Starck) was then deposited on the TiO_2 -coated ZnO NWs to form the p - n heterojunction by spin coating. Finally, 150 nm of gold was deposited by electron-gun evaporation through a shadow mask to provide contact for hole injection.

III. RESULTS AND DISCUSSION

The schematic diagram of the TiO_2/ZnO coaxial NWs/PEDOT:PSS heterostructure LED is shown in Fig. 1(a). The morphology of the TiO_2/ZnO coaxial NWs/PEDOT:PSS heterostructure was examined using field-emission scanning electron microscopy [(FESEM), LEO 1530]. Figure 1(b) shows the top-view image of the as-grown ZnO NWs. The ZnO NWs form a well organized hexagonal shape with a diameter of 70–100 nm. Figure 1(c) shows the cross-sectional image of the TiO_2/ZnO coaxial NWs/PEDOT:PSS heterostructure. The thicknesses of the TiO_2/ZnO coaxial NW/SOG layer and PEDOT:PSS layer are about 960 and 110 nm, respectively. The image shows that the tips of TiO_2/ZnO coaxial NWs can be covered thoroughly by the PEDOT:PSS layer. An x-ray diffraction (XRD) pattern was used to identify the structure of the ZnO NWs. As shown in Fig. 1(d), several diffraction peaks can be observed at $2\theta = 31.74^\circ, 34.44^\circ, 36.26^\circ, 47.48^\circ, 56.66^\circ,$ and 62.93° , which corresponds with ZnO (100), (002), (101), (102), (110), and (103), respectively.¹⁷ Each peak can be indexed to hexagonal ZnO (Joint Committee for Powder Diffraction Standard card No. 36–1451). This observation suggests that these films are composed of high c -axis oriented ZnO NWs.

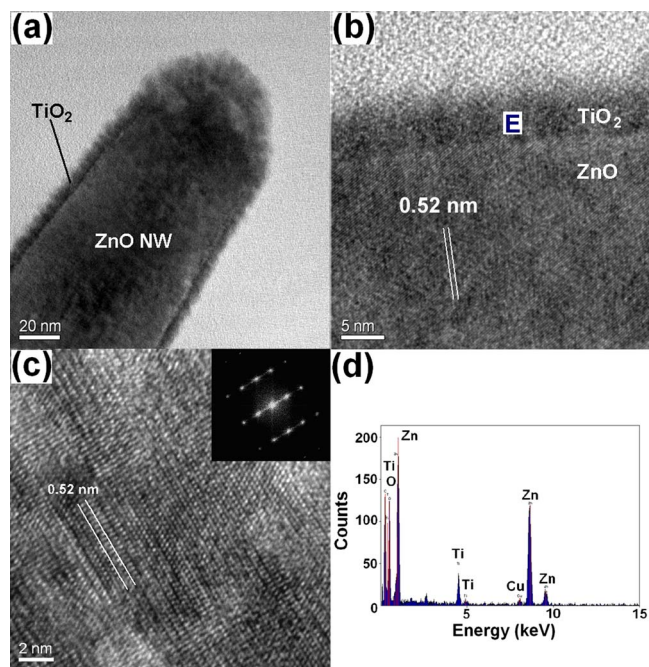


FIG. 2. (Color online) Characterization results of the TiO_2/ZnO coaxial NW. (a) TEM image. (b) The high magnification TEM image. (c) HRTEM image along with the corresponding selected area electron diffraction pattern. (d) EDS spectrum. The coverage of TiO_2 coating was deposited at a current of 40 mA for 150 s.

The TiO_2/ZnO coaxial NW morphology was examined using transmission electron microscopy [(TEM), Philips Tecnai F30] images of a single NW, as shown in Figs. 2(a)–2(c). Here, the TiO_2 coating was deposited by a current of 40 mA for 350 s. It is clear that the deposited TiO_2 coating consists of many nanoclusters, which were referred to as TiO_2 NPs as shown in Fig. 2(a). The thickness of the TiO_2 nanocluster coating on the ZnO NW is about 8–13 nm. In Fig. 2(b), the high-magnification TEM image clearly demonstrates the amorphous formation of the TiO_2 coating layer. The high-resolution TEM (HRTEM) image shown in Fig. 2(c), taken from the NW shown in Fig. 2(a), indicates that the lattice distance, measured from the lattice fringes along the growth axis direction of the ZnO NW, is 0.52 nm. This corresponds to the hexagonal wurtzite structure of ZnO and shows that the preferred growth occurred along the [001] direction.¹⁸ The selected area electron diffraction pattern in the inset exhibits sharply defined spots, indicating that the ZnO NW possesses a single crystal hexagonal structure with good crystalline quality. To further characterize the deposited TiO_2 coating, the composition of the TiO_2 nanocluster, taken from area E in Fig. 2(b) was examined by an energy dispersive x-ray spectrometer. The energy dispersive spectroscopy (EDS) analysis shown in Fig. 2(d) reveals a composition of 60.30% Zn, 27.53% O, and 12.51% Ti, confirming the existence of TiO_2 material.

Figure 3 shows the photoluminescence (PL) spectra of ZnO NWs and TiO_2/ZnO coaxial NWs at a deposition current of 40 mA with different sputtering times. The PL spectra were performed using Jobin Yvon SPEX Fluorolog 3 spectroscope and the excitation source was 325 nm radiation from a 450 W Xe lamp. The uncoated ZnO NWs display a

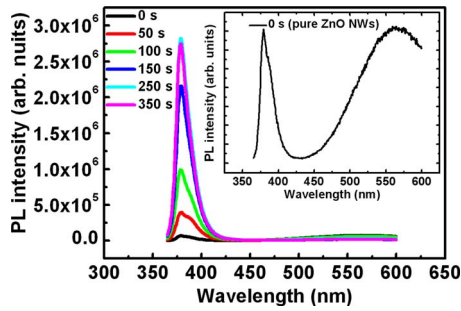


FIG. 3. (Color online) PL spectra of the uncoated ZnO NWs and the TiO_2/ZnO coaxial NWs with different TiO_2 deposition times of 50, 100, 150, 250, and 350 s at a deposition current of 40 mA. The inset shows the enlarged PL spectrum of the uncoated ZnO NWs.

band gap UV emission at 382 nm and a strong defect emission around 560 nm as shown in the inset of Fig. 3. The defect emission arises from oxygen vacancies localized at the ZnO surface.^{19–21} After sputtering the TiO_2 coating, giant enhancements in the band gap emission are observed and the defect emissions are suppressed to the noise level.

This enhancement is based on fluorescence resonance energy transfer (FRET) between the band edge transition of ZnO NWs and TiO_2 NPs.²² FRET is the nonradiative transfer of photon energy from an excited donor to an acceptor located within close proximity. It is a well known phenomenon in many biological systems.²³ The most important factors for the occurrence of FRET include: (1) The fluorescence emission spectrum of the donor must overlap the absorption or excitation spectrum of the acceptor. (2) Donor and acceptor molecules must be in the close proximity to one another (within 1–10 nm). (3) The transition dipole orientations of the donor and acceptor must be approximately parallel.

In this study's devices because of the strong absorption of TiO_2 NPs in the UV range around 3.3 eV, FRET is very feasible when compounded with ZnO NWs. With the TiO_2 sputtering time of 250 s, the band gap emission could be improved by 42 times its current level. In addition, due to the suppression of defect emission, the PL intensity ratio between the band gap and defect emission could be enhanced by up to 111 times its current level. This behavior implies that after the excitation of electron-hole pairs in TiO_2 NPs, the FRET process allows the energy to contribute directly to the band gap emission of ZnO NWs without passing through the defect channel. Hence, the band gap emission of ZnO NWs is greatly enhanced and the defect emission is reduced to noise level. However, as the coating time reaches 350 s, the PL intensity of the band gap emission decreases. After sputtering too many TiO_2 NPs, the band gap emission could be overwhelmed by the high density of TiO_2 NPs. These results are similar to the previous reports on ZnO NWs with surface modification.^{22,24}

The current-voltage (I - V) characteristics were measured by a source meter (Keithley 2400) under ambient air at room-temperature conditions and without encapsulation. Figure 4(a) displays the averaged I - V characteristics of the ZnO NWs/PEDOT:PSS device and the TiO_2/ZnO coaxial NWs/PEDOT:PSS devices with different sputtering times at a deposition current of 40 mA are presented. The figure shows

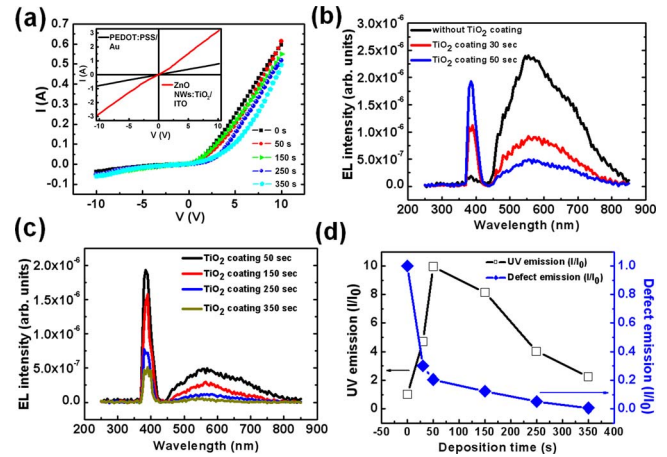


FIG. 4. (Color online) (a) The room temperature I - V characteristics of the ZnO NWs/PEDOT:PSS devices and the TiO_2/ZnO coaxial NWs/PEDOT:PSS devices with different TiO_2 deposition times of 50, 150, 250, and 350 s. (b) EL spectra of the ZnO NWs/PEDOT:PSS device and the TiO_2/ZnO coaxial NWs/PEDOT:PSS devices with different TiO_2 deposition times of 30 and 50 s. (c) EL spectra of the TiO_2/ZnO coaxial NWs/PEDOT:PSS devices with different TiO_2 deposition times of 50, 150, 250, and 350 s. (d) The variation in EL intensity ratio of the band gap and defect emission with different TiO_2 deposition times. The coverage of TiO_2 coating was deposited at a current of 40 mA. The inset of Fig. 4(a) shows the surface I - V curves of the Au and the ITO contacts on the PEDOT:PSS and TiO_2/ZnO coaxial NWs films, respectively.

that all the obtained heterostructure devices exhibit good rectifying behavior of typical p - n junction. It is interesting to note that the slopes of I - V characteristics are different, possibly because of the presence of the TiO_2 coating on the surface of the ZnO NWs. The inset of Fig. 4(a) shows the surface I - V curves of the Au and the ITO contacts on the PEDOT:PSS and TiO_2/ZnO coaxial NWs films, respectively. The linear I - V dependencies reveal that Ohmic contacts have been obtained in both cases. These findings show that the rectifying characteristics presented in Fig. 4(a) resulted from the p - n junction of the NWs/PEDOT:PSS and not to the PEDOT:PSS/Au or ZnO/ITO contacts.

The EL measurements were characterized by a photomultiplier tube (HAMAMATSU, R928) attached to a monochromator (CM110) at room-temperature under forward dc bias of 10 V. Figure 4(b) shows the EL spectra of the ZnO NWs/PEDOT:PSS and TiO_2/ZnO coaxial NWs/PEDOT:PSS devices with different sputtering times of 30 and 50 s at a deposition current of 40 mA. The uncoated ZnO NWs/PEDOT:PSS device exhibits a weak band gap UV emission at 380 nm, and a relatively strong defect emission at 560 nm. Quite remarkably, as the TiO_2 coating is sputtered on the ZnO NWs, the EL spectra of the TiO_2/ZnO coaxial NWs/PEDOT:PSS devices display a very strong enhancement in the band gap emission and reduction in the defect emission. The longer the sputtering time (50 s), the greater the enhancement factor of the band gap emission and the suppression factor of the defect emission. This increase and decrease can be attributed to surface modification by the TiO_2 coating sputtered on ZnO NWs. After TiO_2 NPs are deposited on the surface of ZnO NWs, they can passivate the oxygen vacancies and change the defect structure. As a result, the surface defect is unable to trap carriers again, thus the defect emis-

sion is suppressed. Meanwhile, more electrons in the conduction band combine with the holes in the valence band, thereby enhancing the band gap emission. Therefore, surface modification of defect structures seems to be a plausible explanation responsible for the observed EL enhancement.

However, after a more careful examination of this study's measurement, it is difficult to verify the results shown in Fig. 4(c). The suppression of both the band gap and defect emissions is observed with the further increasing of the coating time (for coating times greater than 50 s) at the same deposition current. In order to provide a more detailed understanding of the influence of the TiO₂ coating, Fig. 4(d) shows the variation in EL intensity ratio of the band gap and defect emissions with different sputtering times. For all different TiO₂ deposition times, increased coating times result in reduced defect emission. The defect emission declines rapidly with deposition time in the first 50 s, and then decreases gradually to the noise level with greater deposition times. In contrast, the band gap emission rises rapidly within the first 50 s. It maximizes at the TiO₂ deposition time of 50 s and then starts to decline gradually with greater deposition times.

The involved mechanism can be understood according to several aspects. When the coating time increases during the first 50 s, this study's results are similar to those of studies of surface modification in PL measurement.^{25,26} During the deposition process of TiO₂ coating on ZnO NWs, TiO₂ NPs can interact with surface defects of the ZnO NWs. This will change the defect states and lead to the passivation of surface defect activity. This passivation leads to the suppression of defect emission. In addition, carriers confined in the thin TiO₂ layer may also contribute to enhancement of the band gap emission. Carrier confinement in semiconductor heterostructure is very useful for the fabrication of high efficiency LEDs.²⁷ Since the TiO₂ layer is very thin (<10 nm), carriers can be confined within this coating layer. Through the energy transfer to ZnO NW, the carriers confined in the TiO₂ layer enhance the band gap emission of ZnO NWs. Figure 5 provides a band alignment diagram that shows a clear physical picture of the energy transfer process in TiO₂/ZnO coaxial NWs.²⁸⁻³⁰ However, after depositing too many TiO₂ NPs (as

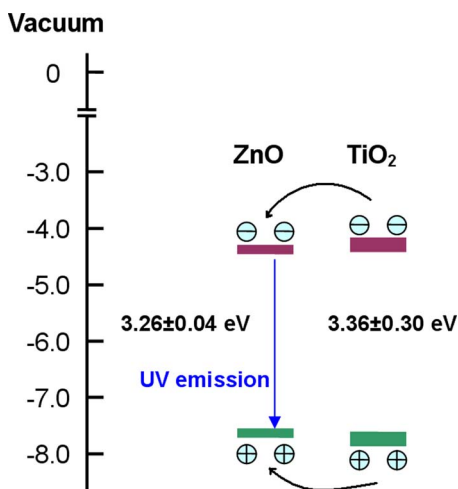


FIG. 5. (Color online) Energy band alignment of TiO₂/ZnO coaxial NW.

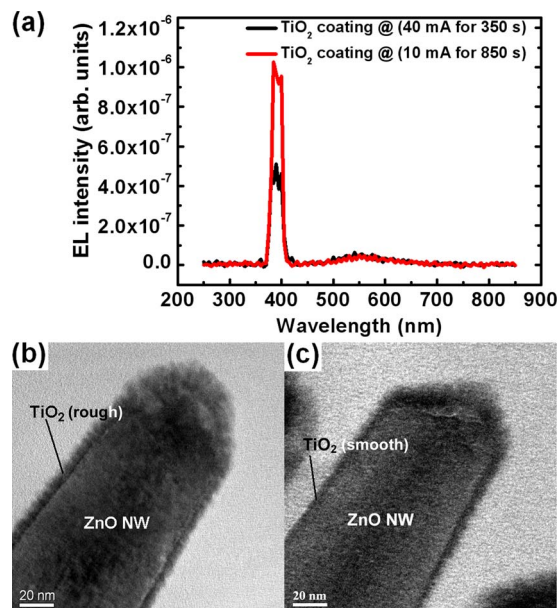


FIG. 6. (Color online) (a) EL spectra of the TiO₂/ZnO coaxial NWs/PEDOT:PSS devices with 8 nm TiO₂ coating at different deposition currents of 40 mA for 350 s and 10 mA for 850 s. The TEM images of the TiO₂/ZnO coaxial NWs with 8 nm TiO₂ coating at different deposition currents of (a) 40 mA for 350 s and (b) 10 mA for 850 s.

the coating time increased beyond 50 s), the NP aggregation form pinhole defects on the surface of the ZnO NWs. These pinhole defects trap the carriers in the TiO₂ layer and cause the excitons to quench, resulting in the reduction in detected EL intensities.

To further investigate the influence of the pinhole defects on the EL emission, this study examines the EL spectra of the ZnO EL devices with different concentrations of pinhole defects as shown in Fig. 6(a). The concentrations of pinhole defects were controlled by different deposition currents. Figures 6(b) and 6(c) present the TEM images of the TiO₂/ZnO coaxial NWs with the same 8 nm-thick TiO₂ coating at different deposition currents of 40 mA for 350 s and 10 mA for 850 s, respectively. These figures show that when the deposition current is smaller, the deposited TiO₂ NP layer is smoother and more continuous, consisting of less pinhole defects. Fewer pinhole defects result in a dramatic increase in UV emission. In the device with 10 mA TiO₂ deposition current, the UV emission intensity is enhanced by nearly two times the level of the device with 40 mA TiO₂ deposition current. Furthermore, in the device with 10 mA TiO₂ deposition current, the band gap/defect emission ratio can increase from 0.081 to 20 compared to the device without TiO₂ coating. In other words, the EL intensity ratio between the band gap and defect emission can be greatly enhanced by up to about 250 times its prior level. Therefore, the EL emission intensity can be influenced by the TiO₂ structure on the ZnO NW surface. This study demonstrates that through the application of TiO₂ coating and the decrease in pinhole defects on the ZnO NW surface, it is possible to obtain a highly efficient ZnO UV LED.

IV. CONCLUSION

In conclusion, enhanced UV EL from TiO₂/ZnO coaxial NWs/PEDOT:PSS inorganic/organic heterostructure devices

have been reported. After the application of TiO₂ coating, the optimized device shows an enhanced factor of up to 250 times of the EL intensity ratio between the band gap and defect emission. The underlying mechanism of this approach is based on the surface modification of the sputtered TiO₂ coating and the reduction of the pinhole traps on the surface of ZnO NWs. This approach can be used for many other nanocomposites as a general strategy to create highly efficient solid state emitters.

ACKNOWLEDGMENTS

The authors wish to acknowledge the support of the National Science Council under Contract Nos. NSC 96-2221-E-002-277-MY3, NSC 98-2218-E-002-002, and NSC 97-2221-E-002-039-MY3.

- ¹H. Zhou, J. Fallert, J. Sartor, R. J. B. Dietz, C. Klingshirn, H. Kalt, D. Weissenberger, D. Gerthsen, H. Zeng, and W. Cai, *Appl. Phys. Lett.* **92**, 132112 (2008).
- ²H. E. Unalan, Y. Zhang, P. Hiralal, S. Dalal, D. Chu, G. Eda, K. B. K. Teo, M. Chhowalla, W. I. Milne, and G. A. J. Amaratunga, *Appl. Phys. Lett.* **94**, 163501 (2009).
- ³Y. Y. Xi, Y. F. Hsu, A. B. Djurišić, A. M. C. Ng, W. K. Chan, H. L. Tam, and K. W. Cheah, *Appl. Phys. Lett.* **92**, 113505 (2008).
- ⁴J. P. Richters, T. Voss, L. Wischmeier, I. Rückmann, and J. Gutowski, *Appl. Phys. Lett.* **92**, 011103 (2008).
- ⁵V. A. Fonoberov, K. A. Alim, A. A. Balandin, F. Xiu, and J. Liu, *Phys. Rev. B* **73**, 165317 (2006).
- ⁶J. V. Foreman, J. Li, H. Peng, S. Choi, H. O. Everitt, and J. Liu, *Nano Lett.* **6**, 1126 (2006).
- ⁷Y. L. Wu, A. I. Y. Tok, F. Y. C. Boey, X. T. Zeng, and X. H. Zhang, *Appl. Surf. Sci.* **253**, 5473 (2007).
- ⁸A. Bera and D. Basak, *ACS Appl. Mat. & Interfaces* **1**(9), 2066 (2009).
- ⁹C. C. Lin, H. P. Chen, H. C. Liao, and S. Y. Chen, *Appl. Phys. Lett.* **86**, 183103 (2005).
- ¹⁰J. M. Lin, C. L. Cheng, H. Y. Lin, and Y. F. Chen, *Opt. Lett.* **31**, 3173 (2006).
- ¹¹K. Remashan, D. K. Hwang, S. J. Park, and J. H. Jang, *Jpn. J. Appl. Phys.* **47**, 2848 (2008).
- ¹²J. Li, D. Zhao, X. Meng, Z. Zhang, J. Zhang, D. Shen, Y. Lu, and X. Fan, *J. Phys. Chem. B* **110**, 14685 (2006).
- ¹³L. Shi, Y. Xu, S. Hark, Y. Liu, S. Wang, L. M. Peng, K. Wong, and Q. Li, *Nano Lett.* **7**, 3559 (2007).
- ¹⁴F. Fang, D. X. Zhao, B. H. Li, Z. Z. Zhang, J. Y. Zhang, and D. Z. Shen, *Appl. Phys. Lett.* **93**, 233115 (2008).
- ¹⁵J. P. Richters, T. Voss, D. S. Kim, R. Scholz, and M. Zacharias, *Nanotechnology* **19**, 305202 (2008).
- ¹⁶M. Ohyama, H. Kouzuka, and T. Yoko, *Thin Solid Films* **306**, 78 (1997).
- ¹⁷M. Ghosh, R. Bhattacharyya, and A. K. Raychaudhuri, *Bull. Mater. Sci.* **31**, 283 (2008).
- ¹⁸S. Baruah and J. Dutta, *Sci. Technol. Adv. Mater.* **10**, 013001 (2009).
- ¹⁹A. van Dijken, E. A. Meulenkaamp, D. Vanmaekelbergh, and A. Meilerink, *J. Lumin.* **87–89**, 454 (2000).
- ²⁰N. E. Hsu, W. K. Hung, and Y. F. Chen, *J. Appl. Phys.* **96**, 4671 (2004).
- ²¹K. Vanheusden, W. L. Warren, C. H. Seage, D. R. Tallent, J. A. Voigtang, and B. E. Gnade, *J. Appl. Phys.* **79**, 7983 (1996).
- ²²T. H. Lin, T. T. Chen, C. L. Cheng, H. Y. Lin, and Y. F. Chen, *Opt. Express* **17**, 4342 (2009).
- ²³C. Berney and G. Danuser, *Biophys. J.* **84**, 3992 (2003).
- ²⁴J. M. Lin, H. Y. Lin, C. L. Cheng, and Y. F. Chen, *Nanotechnology* **17**, 4391 (2006).
- ²⁵T. Chen, G. Z. Xing, Z. Zhang, H. Y. Chen, and T. Wu, *Nanotechnology* **19**, 435711 (2008).
- ²⁶S. Z. Li, C. L. Gan, H. Cai, C. L. Yuan, J. Guo, P. S. Lee, and J. Ma, *Appl. Phys. Lett.* **90**, 263106 (2007).
- ²⁷S. J. An and G. C. Yi, *Appl. Phys. Lett.* **91**, 123109 (2007).
- ²⁸M. Grätzel, *Nature (London)* **414**, 338 (2001).
- ²⁹K. Y. Song, Y. T. Kwon, G. J. Choi, and W. I. Lee, *Bull. Korean Chem. Soc.* **20**, 957 (1999).
- ³⁰H. Y. Lin, Y. Y. Chou, C. L. Cheng, and Y. F. Chen, *Opt. Express* **15**, 13832 (2007).